
Graphite-supported Pt_n Cluster Electrocatalysts: Major Change of Active Sites as a Function of the Applied Potential

Julen Munarriz,^[a,b] Zisheng Zhang,^[a] Philippe Sautet,^{*[a,c,d]} Anastassia N. Alexandrova ^{*[a,c]}

[a] Dr. J. Munarriz, Z. Zhang, Prof. P. Sautet, Prof. A. N. Alexandrova
Department of Chemistry and Biochemistry
University of California, Los Angeles
607 Charles E. Young Drive, Los Angeles, CA 90095-1569 (USA)
E-mail: sautet@ucla.edu, ana@ucla.edu

[b] Dr. J. Munarriz
Departamento de Química Física y Analítica
Universidad de Oviedo
Julián Clavería n° 8, Campus Universitario de El Cristo Oviedo, 33006 (Spain)

[c] Prof. P. Sautet, Prof. A. N. Alexandrova
California NanoSystem Institute
University of California, Los Angeles
607 Charles E. Young Drive, Los Angeles, CA 90095-1569 (USA)

[d] Prof. P. Sautet
Department of Chemical and Biomolecular Engineering
University of California, Los Angeles
5531 Boelter Hall, Los Angeles, California 90095 (USA)

Supporting information for this article is given via a link at the end of the document.

Abstract: The oxygen reduction reaction (ORR) plays a key role in renewable energy transformation processes. Unfortunately, it is inherently sluggish, which greatly limits its industrial application. Sub-nano cluster decorated electrode interfaces are promising candidate ORR electrocatalysts. However, understanding the nature of the active sites on these catalysts in electrocatalytic conditions presents a formidable challenge for both experiment and theory, due to their dynamic fluxional character. Here, we combine global optimization with the electronic Grand Canonical DFT, to elucidate the structure and dynamics of sub-nano Pt_n clusters deposited on electrified graphite. We show that under electrochemical conditions, these clusters exist as statistical ensembles of multiple states, whose fluxionality is greatly affected by the applied potential, electrolyte, and adsorbate coverage. The results reveal the presence of potential-dependent active sites, and hence, reaction energetics.

Introduction

The progressive fossil fuels depletion in conjunction with the need for reducing environmental pollution has motivated an increasing interest in the search for renewable and efficient energy processes.^[1] Within this context, electrocatalysis plays a crucial role, being at the heart of many state-of-the-art energy technologies such as hydro-gen producing devices,^[2] photovoltaic systems^[3] and fuel cells.^[4] Specifically, (sub-nano) Pt-based clusters are promising catalysts for important electrocatalytic process such as the Oxygen Reduction Reaction (ORR).^[5-10] These systems exhibit many intriguing features. For example, the activity and selectivity of size-selected Pt_n (n = 1-14) clusters deposited on glassy carbon and indium tin oxide strongly and non-monotonically depend on the cluster size.^[11-15] One key feature of supported Pt_n clusters is their high fluxional character, which leads to various competing low energy structures. This

results in their capability to change shape from thermal fluctuations, and to restructure in response to the number and nature of the adsorbates. One consequence is that they can circumvent the generally accepted scaling relations of ORR.^[16-18] In electrochemical processes, the catalytic interface can be highly impacted by the applied potential. For example, Reuter and co-workers showed from first principles that the electrode potential causes reconstruction of IrO₂ nanoparticles.^[19] Roldan *et al.* showed a significant restructuring of Cu nanoparticles in CO₂ electro-reduction conditions.^[20] Many catalytic intermediates also exhibit potential-dependent coordination modes, such as pyridine on Au(111),^[21] oxalate on Ni(111),^[22] and activated CO₂ on Cu(211).^[23] These observations, in conjunction with the high fluxionality, and structural sensitivity of Pt clusters to the reaction conditions,^[24] are suggestive of a) several structures and hence active sites present in one chosen electrochemical condition and b) a strong dependence of these available active site(s) on the electrochemical conditions on a cluster-decorated interface. Notice that, at an electrochemical interface, the number of electrons is not fixed, as the electrode acts as a source (cathode) or sink (anode) of electrons. Instead, the electrochemical potential stays constant along the reaction coordinate. Sub-nano clusters are, as other molecular systems, known to adopt different shapes in their different charge state (cationic, neutral, or anionic). Thus, we expect that the explicitly included electrochemical potential should produce significant alterations of the cluster-decorated electrocatalytic interface; as pointed out by us in a recent exploratory work.^[25] The central goal of this study is the elucidation of the structural evolution, reagent coverage, and resultant ORR activity of sub-nano Pt clusters deposited on graphite (as a model system for carbon-based supports), under ORR conditions of applied potential and in the presence of various adsorbate coverages.

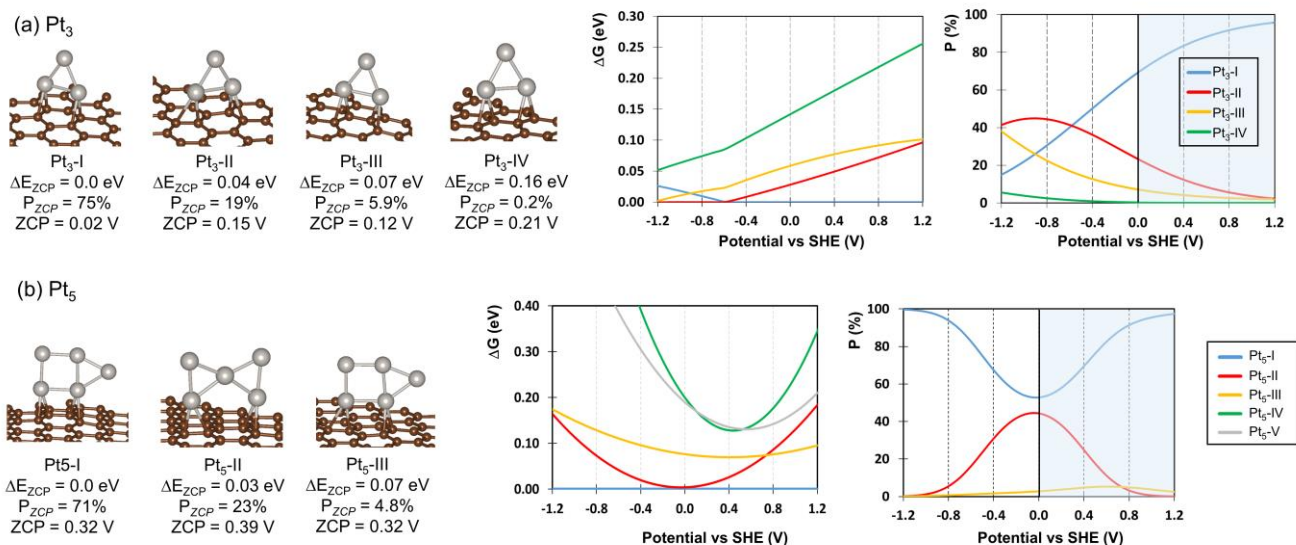


Figure 1. Left: Selected local minima, relative energy with respect to the GM for the zero-charge systems (ΔE_{ZCP}), electrochemical potential associated to the zero-charge system (zero-charge potential, ZCP), and Boltzmann cluster population at 300 K considering the relative energies of the ZCP (P_{ZCP}). Right: ΔG (with respect to the GM at each potential) as a function of the potential (*w.r.t.* SHE), and Boltzmann cluster distribution as a function of the potential, at 300 K in the SC

The methodology suitable for this task requires a special note. While previous studies addressed ORR on graphite/graphene-supported Pt clusters,^[26-30] the global optimization typically required for small clusters has not been accomplished under electrochemical conditions (with the exception of ref. 25). At this point, we should comment on the work of Nakajima and co-workers, who have studied graphite-based surfaces decorated with Pt_n clusters by pre-optimizing the clusters in the gas phase and then depositing them in the surface, the potential effect being later included by means of the Computational Hydrogen Electrode (see below). In order to identify the relevant clusters at working conditions, they relied on XAFS spectroscopy, and used it to match the observations with some of the DFT computed structures.^[15,31] Even though their approach is, without any doubt, valuable, they had to recur to experimental evidence to identify the global minimum (GM), and did not consider ensemble effects. In this sense, our perspective is different, as it is enforced to extract the chemical information from the system without requiring external input.

Indeed, accounting for the potential-dependent effects in adsorption and especially fluxionality is not trivial, and cannot be done, for example, within the widely-used Computational Hydrogen Electrode (CHE) model.^[32] In this work, we therefore combine global optimization techniques with an explicit grand canonical modelling of the electrochemical potential. This is attained by the Surface Charging (SC) method,^[33] which consists of tuning the system workfunction by adding/removing electrons to/from the neutral system. Adding full explicit solvation and the sufficient statistical mechanical sampling of the solvent and ions to the scheme would be prohibitively expensive.^[34] Therefore, we resort to implicit solvation with the linearized Poisson-Boltzmann (PB) model of the electrolyte^[35] - the approach has demonstrated success for a variety of electrochemical processes.^[21,36,37] Note that modelling the electrochemical reconstruction of interfaces is very challenging, and new theoretical methods continue to be developed.^[38-40] We believe our approach is innovative and can offer a significant advance in the understanding of dynamic electrochemical catalytic interfaces.

Results and Discussion

The structures for the global optimizations were generated by our in-house code, PGOPT, with bond length distribution algorithm (BLDA),^[41] and optimized with dispersion-corrected DFT in the presence of an electrostatic potential (with respect to the standard hydrogen electrode), $U(SHE)$. We selected an electrolyte concentration of 1 M and analyzed the electrochemical potential in the [0 - 1.2] V range. We start with the potential dependence of bare clusters, the presence of adsorbates being presented later. We provide the results for the bare clusters at negative potentials just for illustrative (academic) purposes, as for $U(SHE) < 0$ V, they are expected to be covered by hydrogen. The full description of the computational details is provided in the Supporting Information.

Pt₁ and Pt₂ clusters.

Pt₁ and Pt₂ clusters over a graphite surface are considered first. All the initial structures of Pt₁ converged to the same minimum, in which Pt is in the bridging position over a single C-C bond (Figure S1a). This adsorption mode has been reported by other authors.^[26,42] For Pt₂ structures, we also found a single predominant coordination mode, in which the Pt atoms lie over two C-C bonds belonging to adjacent hexagonal rings (Figure S1b). The predicted potential dependence of these structures is minimal.

Pt₃ clusters

Pt₃ clusters have a more diverse conformational distribution: Five different local minima were found within the energy cutoff with respect to the GM of 0.7 eV, when no applied potential is included.

The energy cutoff was chosen generously to account for the possible differential (de)stabilization of the isomers when the potential is applied. The various structures are labeled as Pt₃-#min, where #min indicates the stability order with respect to the GM when the potential effect is not considered (zero-charge system), and this nomenclature is kept for the following systems. All the structures are Pt triangles, whose dimensions and adsorption sites on the support differ slightly (Figure 1a). The four most stable structures are within less than 0.2 eV from the GM. Pt₃-V is significantly less stable than the other isomers, and, even when the potential effect is considered, it does not contribute to the overall Boltzmann ensemble at room temperature.

Isomers Pt₃-I–Pt₃-IV exhibit sensitivity and order switching as a function of the applied potential. Note that, under CHE, the energy difference between the minima would be constant (and equal to that of the zero-charge system), and their statistical distribution would not change as a function of the potential. This way, the Boltzmann structural ensemble would consist of 75% of Pt₃-I, 19% of Pt₃-II and so on; see P_{ZCP} entry in Figure 1 – P_{ZCP} corresponds to the zero-charge potential (ZCP), that is, the results for the neutral systems, which is the basis of the CHE model. In contrast, when we explicitly account for the potential via SC, the picture changes dramatically. For example, the distribution of Pt₃-I now varies as a function of the potential, between 15 and 96% at 300 K, which is a typical temperature in electrocatalysis (see Figure 1). We note that the ability to fully rearrange into an equilibrium thermodynamic ensemble in response to the current conditions is assumed in this study, supported by previous theoretical and experimental findings.^[43,44]

Remarkably, a potential-dependent switch in the GM, between Pt₃-I and Pt₃-II, is observed at -0.6 V. Even though at U(*SHE*) > -0.6 V the GM remains unchanged (as Pt₃-I), the 300 K populations of various isomers (Pt₃-I to Pt₃-III) change as a function of U(*SHE*) (Figure 1a). In fact, no isomer is fully predominant at any potential, and the ensemble composition can be modified by switching the potential. For example, at 0.3 V the ensemble contains 80% of Pt₃-I, 15% of Pt₃-II and 5% of Pt₃-III. While in this case the structures are relatively similar, these results are relevant, as they show the important effect of the applied potential in governing the cluster probability distribution. This GM switch is, in broad strokes, a consequence of the ZCP difference between the various isomers (i.e. 0.02 V for Pt₃-I and 0.15 V for Pt₃-II), which determines the center of the parabolic dependence of the cluster Gibbs energy *w.r.t.* the potential, as the parabola’s curvature (related to the system polarizability, Figure S3) are qualitatively similar. The ZCP changes even further for larger and more geometrically diverse clusters (*vide infra*).

Pt₅ clusters

The Pt₄/graphite system was addressed in a recent separate study.^[25] Pt₅ clusters show a growing geometric diversity (Figure 1b and Figure S4). Pt₅-I (and also Pt₅-III) exhibits distorted pentagonal geometries, which have previously been attributed to a second order Jahn–Teller effect,^[45] hinting at the sensitivity of its stability to the electron count. Indeed, the populations for Pt₅-I and Pt₅-II range between 53-100% and 0.1-44%, respectively, at 300 K (Figure 1b), following the large variations in the energy gap between these structures with the change of the potential. For instance, at 0.0 V, when Pt₅-II is stabilized the most, it is less than 0.01 eV above Pt₅-I, which corresponds to 44% of Pt₅-II and 53%

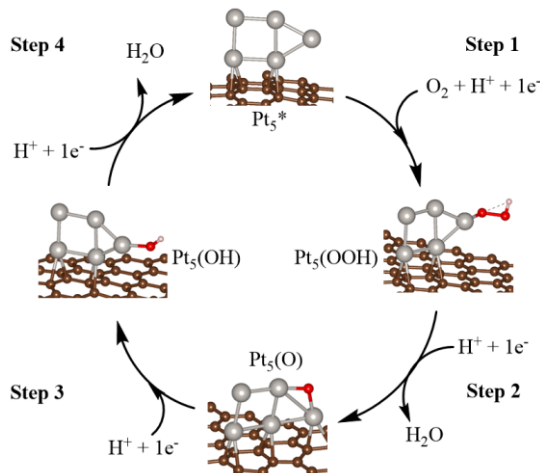
of Pt₅-I. Note that there is a region of the potential of a significant co-existence of Pt₅-I, Pt₅-II and Pt₅-III at 300 K at about 0.7 V. It might seem surprising that Pt₅-I is stabilized at both, more positive and more negative potentials. As shown in Figure S5, it is a consequence of the very different curvature of the Gibbs energy *vs* potential parabolic fitting, which is much higher for Pt₅-I. Again, considering the energy data at the ZCP (CHE model), the populations would stay constant, at 71% of Pt₅-I and 23% of Pt₅-II.

It is noticeable that Pt₅-II (or a closely related structure), has been previously identified for Pt₅ clusters over glassy carbon (while our model support is graphite) by XAFS.^[15] Even though this structure is not the GM in our ensemble at any potential, it further supports our approach.

Potential- and coverage-dependent ORR energetics

on Pt₅/graphite

We now focus on the largest cluster considered in this study, Pt₅/graphite, and report on the impact of the potential and adsorbate coverage effects on the ORR activity. First, we study the adsorption of the reaction intermediates for the 4-electron ORR mechanism (Scheme 1), *O, *OH, and *OOH.^[46] Note that adsorption can be coupled to geometric rearrangements of the cluster, beyond simple relaxation, leading to the reagent itself preparing the real active site possibly absent on the bare catalyst.^[16,47-49] Hence, we aim to interrogate how the nature of the active sites changes as a function of the nature and coverage of the bound intermediates, as well as the applied potential, simultaneously.



Scheme 1. Schematic representation of the four-electron mechanism of ORR. A model Pt₅ cluster with a single adsorbate has been taken as reference for visual purposes.

Pt₅ clusters with one adsorbate

Adding one adsorbate dramatically affects the structural morphology of Pt₅ on graphite. Importantly, the cluster geometry is also potential-dependent (Figure 2). For all three considered

adsorbates, OH, O, OOH, the ensemble at 300 K is composed mainly of two different cluster isomers, with potential-dependent proportions.

For $\text{Pt}_5(\text{OH})$ clusters, we found a potential-dependent GM: $\text{Pt}_5(\text{OH})\text{-I}$ or $\text{Pt}_5(\text{OH})\text{-IV}$. Although the neutral $\text{Pt}_5(\text{OH})\text{-IV}$ is 0.29 eV above the GM (being the fourth most stable geometry), the ZCP for $\text{Pt}_5(\text{OH})\text{-I}$ and $\text{Pt}_5(\text{OH})\text{-IV}$ are very different (0.26 and 0.04 V, respectively), and the curvatures in the parabola are also different (Figure S7). As a result, $\text{Pt}_5(\text{OH})\text{-IV}$ becomes dominant at 1.1 V. On the contrary, zero-charge results (CHE model) would lead to 99% of $\text{Pt}_5(\text{OH})\text{-I}$, 1% of $\text{Pt}_5(\text{OH})\text{-II}$, and no relevant proportions of $\text{Pt}_5(\text{OH})\text{-IV}$ (at 300 K).

For Pt_5O clusters, two structures ($\text{Pt}_5\text{O}\text{-I}$ and $\text{Pt}_5\text{O}\text{-II}$, Figure 2) are very close in energy, with an energy difference of 0.04 eV for the neutral systems, corresponding to 85% of $\text{Pt}_5\text{O}\text{-I}$ and 15% of $\text{Pt}_5\text{O}\text{-II}$. Importantly, the SC modelling of the potential induces two switches in the GM, alternating between these two structures

(see Figure 2). The double switch is a consequence of the parabolic shape of the Gibbs energy with the potential, which in this case translates into $\text{Pt}_5(\text{O})\text{-I}$ being predominant in the [0.1 - 0.8] V range, and $\text{Pt}_5(\text{O})\text{-II}$ outside of this range. This behaviour is attributed to the significantly different values of ZCP, but especially to the very different parabola curvature (*i.e.* in the capacitance variation of these clusters), which is much more pronounced for $\text{Pt}_5(\text{O})\text{-I}$ (see Figure S9).

The same behaviour of alternation between two structures is obtained for $\text{Pt}_5(\text{OOH})$ clusters, with two minima, $\text{Pt}_5(\text{OOH})\text{-I}$ and $\text{Pt}_5(\text{OOH})\text{-II}$ (Figure 2), with an energy difference of only 0.07 eV when the potential effect is not taken into account, which corresponds to 94% of $\text{Pt}_5(\text{OOH})\text{-I}$ and 6% of $\text{Pt}_5(\text{OOH})\text{-II}$ at 300K. Inclusion of the potential via SC changes the picture: in the [0.0-1.2] V range, the $\text{Pt}_5(\text{OOH})\text{-I}$ population varies from 0.1% to 94% (reaching it at *ca.* 0.4 V), and that of $\text{Pt}_5(\text{OOH})\text{-II}$ ranges between 6 and 100% (which is reached at about 1.1 V, see Figure

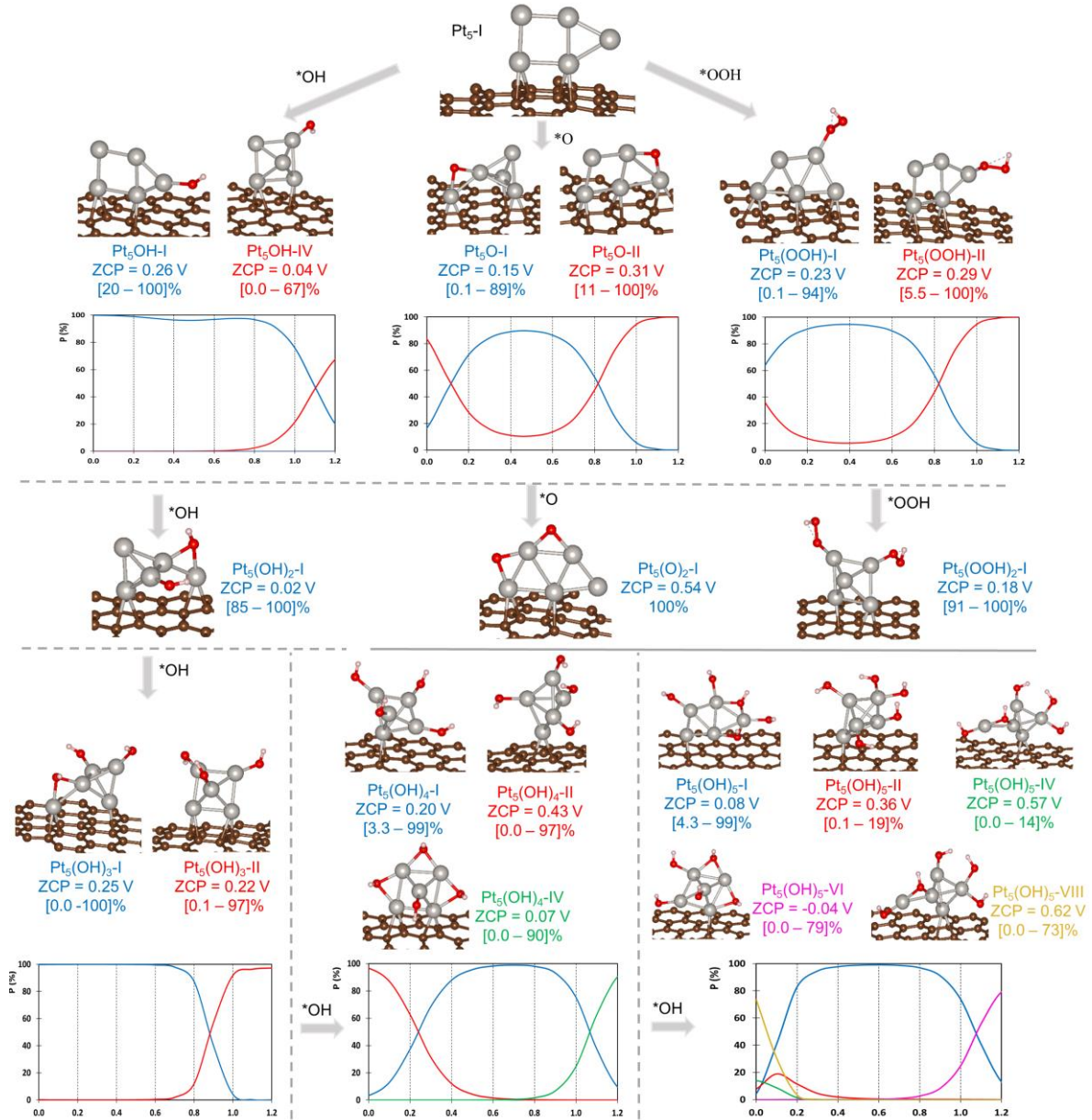


Figure 2. Selected local minima for Pt_5 -adsorbate systems, ZCP and Boltzmann cluster distribution as a function of the potential in the SC framework at 300 K. The x axis corresponds to the potentials (vs SHE) in unit of V.

2). There is a GM switch from Pt₅(OOH)-I to Pt₅(OOH)-II at *ca.* 0.8 V. As for Pt₅(O), the GM switch is a consequence of the very different parabola curvatures (see Figure S11).

Pt₅ clusters with two adsorbates

Interestingly, additional adsorbates change the GM, and that is especially significant for Pt₅(OOH)₂ and Pt₅(OH)₂ (Figure 2), whose geometrical structures are completely different from those of Pt₅(OOH) and Pt₅(OH). For OH, the preferred binding mode also changes from atop to bridge. Contrarily to the previous case, the GM is constant in the entire potential range: 100% of Pt₅(O)₂ is in Pt₅(O)₂-I, and 96-100% of Pt₅(OOH)₂ is in Pt₅(OOH)₂-I. The collapse of the ensemble to a single structure is a signature of particular stability, reached through adsorbate-induced geometric change, and making the adsorption stronger.^[50] The potential-dependent geometric variation is somewhat more pronounced for Pt₅(OH)₂, where the population of GM, Pt₅(OH)₂-I, oscillates between 85 and 100%. Due to lower structural variation with the potential, the results in this case would be closer to those of the CHE model, which predicts populations of Pt₅(OOH)₂-I, Pt₅(O)₂-I and Pt₅(OH)₂-I of 92%, 100% and 96% at 300 K.

Pt₅ clusters with three, four and five OH adsorbates

As will be shown below, the analysis of the ORR energetics reveals the fourth step (protonation of *OH to yield water) being thermodynamically limiting. This is because the *OH binding is the most exothermic for one and two adsorbates (Figure 3), which would lead to the clusters at the catalytic interface being covered by the *OH adsorbates.^[46] Hence, we focus on *OH and increase the adsorbate coverage. The third *OH adsorbate reinvigorates the potential-dependence of the GM. At ZCP Pt₅(OH)₃-I is 0.20 eV more stable than Pt₅(OH)₃-II, which corresponds to relative proportions of 99.9 and 0.05%, respectively, at 300 K. However, in the more realistic SC framework, GM switches at 0.9 V from Pt₅(OH)₃-I (structurally related to Pt₅(OH)₂-I) to Pt₅(OH)₃-II. Contrarily to other cases, in which GM switches were associated to significantly different ZCPs, in this case the two structures have very similar values ZCPs of 0.25 and 0.22 V. Nonetheless, the capacitances are very different, as revealed by a significantly higher curvature in the parabola for Pt₅(OH)₃-II (see Figure S16), which is responsible of it being more stable from 0.9 V on.

The addition of a fourth *OH adsorbate also brings important consequences for the ensemble composition. GM changes three times as a function of the potential in the studied widow. The GM at ZCP, Pt₅(OH)₄-I, is predominant in the [0.25 – 1.1] V range, Pt₅(OH)₄-II is GM up to 0.25 V, and Pt₅(OH)₄-IV is GM at potential above 1.1 V. Notice that the structural diversity of clusters geometry is reflected in the electrochemical behaviour; namely, ZCP varies in a wide range (0.20 V for Pt₅(OH)₄-I, 0.43 V for Pt₅(OH)₄-II and 0.07 V for Pt₅(OH)₄-III), which, in conjunction with different parabola curvatures (Figure S18), results in the aforementioned stability alteration. The ensemble composition in the CHE picture would be 86% of Pt₅(OH)₄-I and 13% of Pt₅(OH)₄-II at all potentials at 300 K.

Finally, Pt₅(OH)₅ clusters also exhibit a strong geometric dependence on the applied potential (Figure 2 bottom right). Namely, in the [0.0 – 1.2] V range, there are three main predominance regions: [0.0 – 0.1], [0.1 – 1.0] and [1.0 – 1.2] V.

Between 0 and 0.1 V, Pt₅(OH)₅-VIII is majority, with 73% population at 0 V. Other significant structures in this range are the GM at ZCP (Pt₅(OH)₅-I), as well as Pt₅(OH)₅-II and Pt₅(OH)₅-VI. Note that, while Pt₅(OH)₅-VIII is 0.23 eV higher in energy than the GM, their ZCP values are very different (0.08 V for Pt₅(OH)₅-I and 0.64 V for Pt₅(OH)₅-VIII, Figure 2 bottom right), which, in conjunction with a different curvature in the parabola is responsible for the switch in the potential-dependent GM (Figure S20). In addition, when inspecting Figure 2, it is clear that Pt₅(OH)₅-VI and Pt₅(OH)₅-VIII show very similar geometries, only exhibiting subtle differences in interatomic distances, namely at ZCP Pt₅(OH)₅-VI is only 0.02 eV more stable than Pt₅(OH)₅-VIII. This way, when including the potential effect via SC, the combination of ZCP and parabola’s curvature translates in Pt₅(OH)₅-VIII being more stable in the considered range. Between 0.1 and 1.0 V, Pt₅(OH)₅-I, constitutes the majority; while at potentials above 1.0 V, Pt₅(OH)₅-VI does. This is mainly attributed to a sharper parabola curvature for Pt₅(OH)₅-VI (Figure S20). One complication here is that with 5 adsorbates, we start finding cluster geometries which are less bonded to the support. This might indicate the high propensity for sintering, affecting the practicability of ORR catalysis on Pt_n/graphite.

The populations at 300 K derived from the CHE approach are: 94% of Pt₅(OH)₅-I, 5% of Pt₅(OH)₅-II, 0.3% of Pt₅(OH)₅-III, and only 0.1% of other clusters; which reveals the large sensitivity of the ensemble composition of the adsorbate decorated electrocatalysts to the applied potential.

ORR electrocatalysis on Pt₅/graphite

We now explicitly address the energetics of the ORR steps, with the special focus on the potential limiting reaction step (step 4 in Scheme 1). The following discussion is based on the system ensemble-averaged adsorption energies (Figure 3), but qualitatively similar conclusions can be drawn when the energies are computed with respect to the GM at each potential (see Figure S21). We first consider one adsorbate, ensemble binding energies of *O, *OH, and *OOH (\boxtimes G_O, \boxtimes G_{OH}, and \boxtimes G_{OOH}) to Pt₅ being shown in Figure 3a. *OOH shows the least favourable binding, between 2.63 and 3.18 eV (versus 3.14 eV in the CHE framework). Notice that \boxtimes G_{OOH} exhibits a “shoulder” at about [0.8 – 1.2] V, due to the GM switching from Pt₅(OOH)-I to Pt₅(OOH)-II in this region, which affects the relative cluster proportions, and thus the total ensemble energy of the system. \boxtimes G_O are in the range between 0.71 and 0.78 eV (versus 0.72 eV in the CHE framework). Remarkably, \boxtimes G_{OH} is negative, -0.18 eV in CHE, and between -0.13 and -0.21 eV in SC, revealing that Pt₅/graphite suffers from over-binding, which is expected to limit the ORR activity and will lead to the catalytic interface being covered of *OH adsorbates.^[25] Based on adsorption energies, we computed \boxtimes G for the four steps of ORR (Scheme 1, \boxtimes G₁ – \boxtimes G₄) as a function of the potential (right-hand side of Figure 3a). Due to *OH over-binding, \boxtimes G₄ (protonation of *OH to produce water) is the thermodynamically limiting step of ORR, being positive in the entire potential range, [0 – 1.2] V.^[15,25,51] This would suggest that Pt₅/graphite is inactive towards ORR catalysis in the considered coverage conditions; as \boxtimes G₄ becomes negative at about -0.1 V, which would correspond to an ORR overpotential higher than 1.23 V. This result resonates with previous calculations on Pt₅, which, under an already explained different approach predicted an overpotential of 1.04 V.^[15]

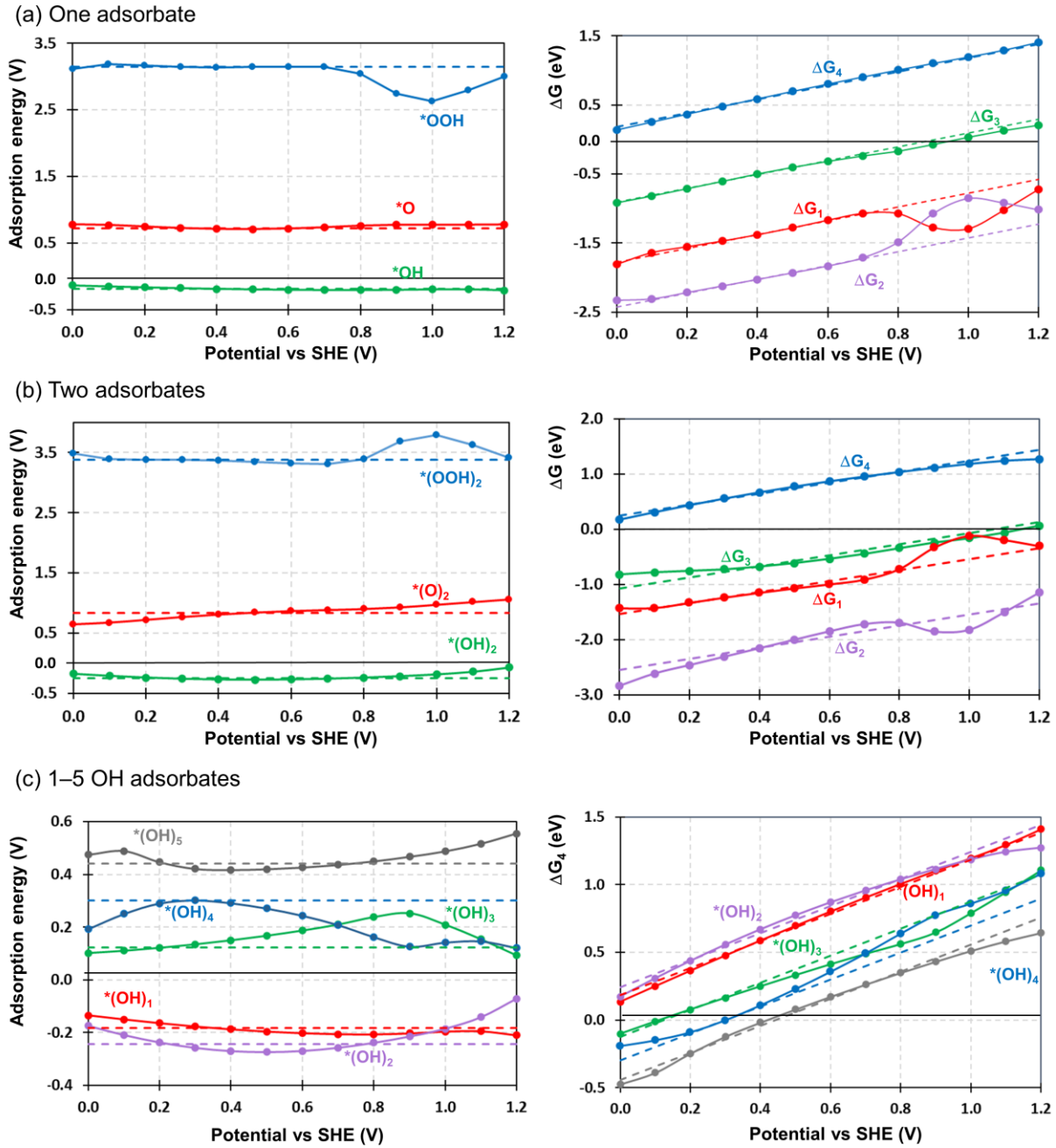


Figure 3. (a) Binding energy of one adsorbate (*O , *OH and *OOH) to Pt_5/C ensemble and ΔG for the four steps of the 4-e⁻ mechanism of ORR. (b) Binding energy of two adsorbates (*O , *OH and *OOH) and ΔG for the four steps of the 4-e⁻ mechanism of ORR. (c) Binding energy of 1 – 5 *OH adsorbates and ΔG_4 for the 4-e⁻ mechanism of ORR. SC results are shown in solid lines and CHE ones in dotted lines.

There are some significant differences between SC and CHE results. While they are almost indistinguishable in the low potential range, the GM switching in $Pt_5(OOH)$ translates into important oscillations in ΔG_1 and ΔG_2 , even leading to them crossing at 1.0 V. At this point, we note that relevant differences between both approaches had also been proposed by some of us.^[46] Next, we study how coverage affects the energetics of the reaction steps. We added an extra *O , *OH and *OOH adsorbate to the previous structures; *i.e.* *OH to $Pt_5(OH)$, *OOH to $Pt_5(OOH)$ and *O to $Pt_5(O)$, and computed the binding energies (*w.r.t.* the previous coverage) and the derived ΔG values for the four steps

of ORR. We found that the absolute values of the binding energies are relatively similar to those computed for a single adsorbate (see Figures 1a and 2a, left-hand side). Unfortunately, ΔG_{OH} is roughly the same (even about 0.05 eV more negative at low potentials) as for $Pt_5(OH)$, indicating that this coverage increase does not mitigate over-binding, and ORR would not take place in the potential range between 0 and 1.23 V (as ΔG_4 is positive, unfavourable in the whole range). Moreover, the negative adsorption energy for *OH , would strengthen the possibility of the real catalytic interface being covered of *OH adsorbates.

This way, as *OH adsorption is by far more favourable than *O and *OOH, and the ORR thermodynamic-limiting reaction step is #4 – *OH protonation to yield water, we only consider further addition of *OH to the cluster catalyst ensemble (Figure 3c). The third *OH leads to a change in both the binding sites and the cluster shape, which is typical of sub-nano cluster catalysis.^[50] This has relevant implications for the energetics of the activity-limiting ORR step. Specifically, ΔG_{OH} is now positive (about 0.2–0.4 eV increase compared to two adsorbates), indicative of partial mitigation of over-binding. This leads to ΔG_4 being negative (favourable) at potentials lower than 0.1 V (which corresponds to an ORR overpotential of 1.12 V, in both CHE and SC approaches). Interestingly, the CHE and SC binding energies (and thus ΔG_4 values) are relatively similar at low potentials (between 0 and 0.3 V, and that is why they lead to similar overpotentials), but differ significantly at potentials higher than 0.3 V. This is a consequence of cluster fluxionality and the parabolic dependence of the system Gibbs energy on the potential.

ORR energetics are even more favourable upon adsorption of the fourth adsorbate, which leads to an additional change in cluster morphology. Interestingly, ΔG_{OH} increases at low potentials, while it is less unfavourable than that derived from three adsorbates at [0.7 – 1.2] V. Notice that ΔG_{OH} in the SC framework deviates significantly from that derived from CHE (see Figure 3c, left-hand side). The increase in ΔG_{OH} at low potentials leads to further decrease in the ORR overpotential. Namely, the ORR onset potential – the potential at which all reaction steps became thermodynamically favourable – would be 0.30 V, corresponding to an overpotential of 0.93 V.

This favourable tendency holds for the fifth adsorbate, which further destabilizes *OH adsorption by about 0.1–0.4 eV (depending on the potential, Figure 3c). This benefits the fourth ORR step, which now becomes exothermic at 0.4 V, that is, the system would have an ORR overpotential of 0.81 V.

Thus, we can see that increasing cluster coverage reduced ORR overpotential, and, although it keeps being higher than that of Pt(111) (about 0.4 V),^[32,52,53] it is indicative of the activity increase. In addition, it should be highlighted that, even though the overpotential of these clusters is higher than that of Pt(111), the Pt loading in this systems is much lower, and the relative surface area and site-specificity to interact with O₂ molecules is higher, which can overcome the overpotential increase in practical applications.^[15,54] Note that adsorption energies of *OH point towards the adsorption of the first two adsorbates being thermodynamically favourable, thus revealing that the real catalytic interface will be covered by OH. The extension to which this coverage takes place would also depend on the experimental conditions (such as electrolyte concentration and temperature), but our results reveal how increasing coverage affects the catalytic activity and that more than one adsorbate needs to be considered to account for the system activity.^[55]

Conclusion

This study reveals that an accurate description of cluster-decorated electrochemical interfaces requires the explicit consideration of the electrochemical potential and the restructuring of the interface at this potential, and in the presence of the adsorbates at relevant coverages. Because of the highly fluxional character of deposited sub-nano clusters, they are able

to change shapes as a function of the applied potential, so that the dominant species in the cluster population also can be highly potential-dependent. We expect the behaviour to be non-monotonic with the Pt cluster size, as Pt₃ and Pt₅ behave differently, and the same happens with different adsorbates coverages for Pt₅ size: some systems show a more pronounced structural sensitivity to the potential. Moreover, the example of Pt₅ with adsorbates highlights the dramatic geometrical change that takes place when adsorbates bind to the clusters in their potential-dependent binding modes. Considering more relevant higher coverages is also evidently crucial for predicting the ORR activity, whereas at lower coverages, the *OH adsorption is too strong and incompatible with the ORR activity. These results have important implications for cluster electrocatalysis and provide a step toward the accurate modelling of electrochemical interfaces, and understanding of novel catalysts with switchable properties a function of the potential.

As a final comment, we should note that parameters in the model can affect the absolute values of binding energies and overpotentials. However, the results highlight important phenomena that must hold true regardless of the model, such as potential-dependent cluster fluxionality and interface restructuring, and, consequently, potential-dependent binding energies and ORR steps energetics (and thus overpotentials).

Acknowledgements

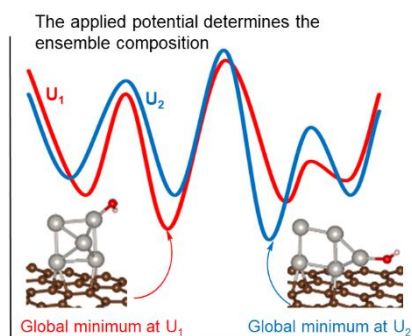
This work was supported by the DOE BES grant DE-SC0020125. The authors acknowledge the computational resources and technical assistance from NERSC, INCITE, and UCLA shared cluster, Hoffman2.

Keywords: Cluster catalysis • Electrochemistry • Fluxionality • Oxygen Reduction Reaction • DFT

- [1] S. Chu, A. Majumdar, *Nature* 2012, *488*, 294–303.
- [2] K. S. Joya, Y. F. Joya, K. Ocakoglu, R. van de Krol, *Angew. Chem. Int. Ed.* 2013, *52*, 10426–10437.
- [3] N. S. Lewis, D. G. Nocera, *Proc. Natl. Acad. Sci. U. S. A.* 2006, *103*, 15729–15735.
- [4] S. Mekhilef, R. Saidur, A. Safari, *Renewable Sustainable Energy Rev.* 2012, *16*, 981–989.
- [5] A. Halder, L. A. Curtiss, A. Fortunelli, S. Vajda, *J. Chem. Phys.* 2018, *148*, 110901.
- [6] A. von Weber, S. L. Anderson, *Acc. Chem. Res.* 2016, *49*, 2632–2639.
- [7] B. Seger, P. V. Kamat, *J. Phys. Chem. C* 2009, *113*, 7990–7995.
- [8] R. Kou, Y. Shao, D. Wang, M. H. Engelhard, J. H. Kwak, J. Wang, V. V. Viswanathan, C. Wang, Y. Lin, Y. Wang, I. A. Aksay, I. J. Liu, *Electrochem. Commun.* 2009, *11*, 954–957.
- [9] B. -W. Zhang, L. Ren, Z. -F. Xu, N. -Y. Cheng, W. -H. Lai, L. Zhang, W. Hao, S. -Q. Chu, Y. -X. Wang, Y. Du, L. K. Liu, S. -X. Dou, *Small* 2021, *2100732*.
- [10] M. Inaba, A. Zana, J. Quinson, F. Bizzotto, C. Dosche, A. Dworzak, M. Oezaslan, S. B. Simonsen, L. T. Kuhn, M. Arenz, *ACS Catal.* 2021, *11*, 7144–7153.
- [11] S. Proch, M. Wirth, H. S. White, S. L. Anderson, *J. Am. Chem. Soc.* 2013, *135*, 3073–3086.
- [12] A. von Weber, E. T. Baxter, S. Proch, M. D. Kane, M. Rosenfelder, H. S. White, S. L. Anderson, *Phys. Chem. Chem. Phys.* 2015, *17*, 17601–17610.
- [13] A. von Weber, E. T. Baxter, H. S. White, S. L. Anderson, *J. Phys. Chem. C* 2015, *119*, 11160–11170.

- [14] J. W. Magee, W. -P. Zhou, M. G. White, *Appl. Catal. B-Environ.* 2014, *152-153*, 397-402.
- [15] A. Ohnuma, K. Takahashi, H. Tsunoyama, T. Inoue, P. Zhao, A. Velloth, M. Ehara, N. Ichikuni, M. Tabuchi, A. Nakajima, *Catal. Sci. Technol.* 2022, *12*, 1400-1407.
- [16] B. Zandkarimi, A. N. Alexandrova, *J. Phys. Chem. Lett.* 2019, *10*, 460-467.
- [17] J. Pérez-Ramírez, N. López, *Nat. Catal.* 2019, *2*, 971-976.
- [18] Z. -F. Huang, J. Song, S. Dou, X. Li, J. Wang, X. Wang, *Matter* 2019, *1*, 1494-1518.
- [19] D. Opalka, C. Scheurer, K. Reuter, *ACS Catal.* 2019, *9*, 4944-4950.
- [20] A. Yoon, J. Poon, P. Grosse, S. W. Chee, B. Roldan Cuenya, *J. Mater. Chem. A* 2022, *10*, 14041-14050.
- [21] S. N. Steinmann, P. Sautet, *J. Phys. Chem. C* 2016, *120*, 5619-5623.
- [22] S. N. Steinmann, C. Michel, R. Schwiedernoch, P. Sautet, *Phys. Chem. Chem. Phys.* 2015, *17*, 13949-13963.
- [23] L. Liu, C. Liu, *Phys. Chem. Chem. Phys.* 2018, *20*, 5756-5765.
- [24] E. T. Baxter, M. -A. Ha, A. C. Cass, A. N. Alexandrova, S. L. Anderson, *ACS Catal.* 2017, *7*, 3322-3335.
- [25] Z. Zhang, B. Zandkarimi, J. Munarriz, C. E. Dickerson, A. N. Alexandrova, *ChemCatChem* 2022, *e202200345*.
- [26] G. Ramos-Sanchez, P. B. Balbuena, *Phys. Chem. Chem. Phys.* 2013, *15*, 11950-11959.
- [27] D. -H. Lim, J. Wilcox, *J. Phys. Chem. C* 2011, *115*, 22742-22747.
- [28] Y. Okamoto, *Chem. Phys. Lett.* 2006, *420*, 382-386.
- [29] Q. Qi, H. Liu, W. Feng, H. Tian, H. Xu, X. Huang, *Comput. Mater. Sci.* 2015, *96*, 268-276.
- [30] J. Ma, A. Habrioux, Y. Luo, G. Ramos-Sanchez, L. Calvillo, G. Granozzi, P. B. Balbuena, N. Alonso-Vante, *J. Mater. Chem. A* 2015, *3*, 11891-11904.
- [31] Tsunoyama, H.; Ohnuma, A.; Takahashi, K.; Velloth, A.; Ehara, M.; Ichikuni, N.; Tabuchi, M.; Nakajima, A. Enhanced oxygen reduction activity of platinum subnanocluster catalysts through charge redistribution. *Chem. Commun.* 2019, *55*, 12603-12606.
- [32] J. K. Nørskov, J. Rossmeisl, A. Logadottir, L. Lindqvist, J. R. Kitchin, T. Bligaard, H. Jónsson, *J. Phys. Chem. B* 2004, *108*, 17886-17892.
- [33] C. D. Taylor, S. A. Wasileski, J. -S. Filhol, M. Neurock, *Phys. Rev. B* 2006, *73*, 165402.
- [34] H. H. Kristoffersen, T. Veggem H. A. Hansen, *Chem. Sci.* 2018, *9*, 6912-6921.
- [35] K. Mathew, R. Sundararaman, K. Letchworth-Weaver, T. A. Arias, R. G. Hennig, *J. Chem. Phys.* 2014, *140*, 084106.
- [36] K. Chang, H. Zhang, J. G. Chen, Q. Liu, M. -J. Cheng, *ACS Catal.* 2019, *9*, 8197-8207.
- [37] J. D. Goodpaster, A. T. Bell, M. Head-Gordon, *J. Phys. Chem. Lett.* 2016, *7*, 1471-1477.
- [38] Y. Basdogan, A. M. Maldonado, J. A. Keith, *WIREs Comput Mol Sci.* 2019, *e1446*.
- [39] J. A. Gauthier, S. Ringe, C. F. Dickens, A. J. Garza, A. T. Bell, M. Head-Gordon, J. K. Nørskov, K. Chan, *ACS Catal.* 2019, *9*, 920-931.
- [40] N. Abidi, K. R. G. Lim, Z. W. Seh, S. N. Steinmann, *WIREs Comput. Mol. Sci.* 2021, *11:e1499*.
- [41] H. Zhai, A. N. Alexandrova, *J. Chem. Theory Comput.* 2016, *12*, 6213-6226.
- [42] M. N. Groves, C. Malardier-Jugroot, M. Jugroot, *J. Phys. Chem. C* 2012, *116*, 10548-10556.
- [43] H. Zhai, A. N. Alexandrova, *J. Phys. Chem. Lett.* 2018, *9*, 1696-1702.
- [44] T. Imaoka, T. Toyonaga, M. Morita, N. Haruta, K. Yamamoto, *Chem. Commun.* 2019, *55*, 4753-4756.
- [45] L. Shen, J. Dadras, A. N. Alexandrova, *Phys. Chem. Chem. Phys.* 2014, *16*, 26436-26442.
- [46] R. Shang, S. N. Steinmann, B. -Q. Xu, P. Sautet, *Catal. Sci. Technol.* 2020, *10*, 1006-1014.
- [47] Z. Zhang, B. Zandkarimi, A. N. Alexandrova, *Acc. Chem. Res.* 2020, *53*, 447-458.
- [48] H. Zhai, A. N. Alexandrova, *ACS Catal.* 2017, *7*, 1905-1911.
- [49] A. Zhang, Z. -H. Cui, E. Jimenez-Izal, P. Sautet, A. N. Alexandrova, *ACS Catal.* 2020, *10*, 13867-13877.
- [50] R. H. Lavroff, H. W. T. Morgan, Z. Zhang, P. Poths, A. N. Alexandrova, *Chem. Sci.* 2022, *13*, 8003-8016.
- [51] H. A. Hansen, V. Viswanathan, J. K. Nørskov, *J. Phys. Chem. C* 2014, *118*, 6706-6718.
- [52] G. Hoogers, D. Thompsett, *CATTECH* 1999, *3*, 106.
- [53] A. Kulkarni, S. Siahrostami, A. Patel, J. K. Nørskov, *Chem. Rev.* 2018, *118*, 2302-2312.
- [54] M. K. Debe, *Nature* 2012, *486*, 43-51.
- [55] Pt₅ clusters over glassy carbon have been found to be active towards ORR, as described in reference 15.

Entry for the Table of Contents



The effect of the applied potential on the ensemble composition of Pt_n ($n = 3, 5$) sub-nano clusters deposited over graphite in the presence of relevant intermediates of ORR is explored by combining global optimization techniques with the electronic Grand Canonical DFT in the Surface Charging framework. The results show that the potential has a major effect on the ensemble composition, revealing the many potential-dependent active sites, which result in a potential-dependent reaction energetics for the ORR.